IRGS Journal of Multidisciplinary Research and Studies
Website: www.irgspublisher.com
Email: office@irgspublisher.com
Vol-1, Iss-1, May-June 2026
ISSN: XXXX-XXXX

Vegetation and Radiative Controls on Urban Heat Islands in Lagos Metropolis, Nigeria (1984–2013): A PCA Approach

Uwadiegwu Ibeabuchi[1], Feyi O. Oni[2], Olusegun A. Adeaga[3]
[1,2,3]Department of Geography, Faculty of Social Science, University of Lagos, Lagos-Nigeria

Article History:
Received: 18/04/2026
Accepted: 15/05/2026
Published: 10/06/2026

Corresponding Author:
Uwadiegwu Ibeabuchi

Abstract

Urbanization modifies the surface energy balance and drives Urban Heat Island (UHI) intensification, yet the quantitative partitioning of radiative, thermal, and vegetation controls remains poorly constrained in rapidly growing tropical megacities. This study quantified spatiotemporal dynamics of Land Surface Temperature (LST), Net Radiation (Rn), Normalized Difference Vegetation Index (NDVI), and urban built-up extent in Lagos metropolis, Nigeria, from 1984 to 2013, and identified latent climatic controls using Principal Component Analysis (PCA) with Varimax rotation. Landsat Thematic Mapper (TM) 5, Enhanced Thematic Mapper Plus (ETM+) 7, and Operational Land Imager (OLI) 8 imagery were processed to retrieve LST via single-channel algorithms, Rn from surface energy balance components, and NDVI from red and near-infrared reflectance. Four variables—urban built-up fraction, LST, Rn, and NDVI—were subjected to PCA. Mean LST in built-up zones increased from 24.76°C in 1984 to 28.59°C in 2013, while NDVI and rural open land declined by 68%. PCA extracted two orthogonal factors accounting for 100.00% of cumulative variance. Factor 1, termed the Radiative-Thermal Factor, exhibited loadings of 0.999 for LST, 0.998 for Rn, and 0.764 for urban built-up fraction, explaining 67.89% of variance. Factor 2, the Vegetation Factor, loaded 0.998 on NDVI and explained 32.11% of variance. The urban–rural LST differential widened from 2.69°C to 4.87°C, and daytime Surface UHI extent expanded from 147.06 km² to 332.36 km². Results indicate that urbanization-induced alterations in radiative balance and vegetation loss constitute the principal controls on Lagos's urban climate. Mitigation should prioritize expansion of green infrastructure, deployment of high-albedo materials, and mandatory UHI impact assessment in high-priority Local Government Areas.

Keywords: Urban Heat Island; Land Surface Temperature; Net Radiation; Principal Component Analysis; Lagos Metropolis

Article Citation: U. Ibeabuchi, F.O. Oni, & O. A. Adeaga (2026). Vegetation and Radiative Controls on Urban Heat Islands in Lagos, Nigeria (1984–2013): A PCA Approach. **IRGS Journal of Multidisciplinary Research and Studies (IRGSJMRS),** Vol-1(Iss-1), 33-42.

1. Introduction

Urbanization concentrates populations in cities and transforms land cover, generating distinct urban climates. When vegetation is replaced by buildings and paved surfaces, surface albedo, thermal inertia, and radiation balance shift, creating microclimates that diverge from adjacent rural zones. This temperature differential is defined as the Urban Heat Island (UHI), with urban areas typically 2–15 °C warmer than surrounding countryside (Aflaki et al., 2017; Mohajerani et al., 2017; Zhao et al., 2016; Santamouris, 2015). Rapidly expanding megacities function as natural laboratories for projecting future climate stresses. Impervious materials absorb and re-emit more solar energy than vegetated or bare soils, amplifying heat accumulation and UHI intensity (He et al., 2021). Surface UHI exhibit marked diurnal variability, with daytime effects exceeding nocturnal effects due to direct solar forcing (Estoque et al., 2017; Athukorala & Murayama, 2021).

As urban populations grow, UHI risks like heat stress, elevated mortality, and deteriorated air quality will intensify (Coumou & Rahmstorf, 2012). UHI also compromise health by straining cardiovascular and respiratory systems and raising heat-related mortality (Rajagopalan et al., 2014; Yang et al., 2016). Warm air over heated surfaces traps pollutants, suppressing dispersion and degrading air quality (Baklanov et al., 2016). Other consequences include altered hydrology, modified microclimates, and reduced outdoor thermal comfort (Oke et al., 2017; Romero, 2011; Gartland & Gonçalves, 2010; Santamouris, 2015).

Urbanization drives these perturbations through soil sealing, albedo reduction, and vegetation loss, which disrupt the surface energy balance (Oke, 1982). Natural surfaces such as vegetation and water bodies store and release less heat than concrete and asphalt, thereby increasing sensible heat flux while reducing latent heat flux and atmospheric humidity (Xian, 2021; Taleghani et al., 2019). Primary mechanisms underlying UHI formation include heat storage in construction materials, anthropogenic heat emissions, diminished wind flow due to surface roughness, and enhanced solar absorption by low-albedo surfaces (Oke et al., 2017; Romero, 2011; Gartland & Gonçalves, 2010; Santamouris, 2015).

Empirical evidence from Lagos metropolis validates these processes. Ibeabuchi et al. (2026) quantified UHI dynamics in Lagos metropolis across three epochs, 1984, 2000, and 2013 using Landsat Thematic Mapper (TM) 5, Enhanced Thematic Mapper Plus (ETM+) 7, and Operational Land Imager (OLI) 8 imagery. Land Surface Temperature (LST) was retrieved from thermal bands, and urban–rural boundaries were delineated by supervised classification. Their results indicate that urban built-up area expanded while vegetated/open land contracted, intensifying UHI. Urban LST rose from 24.76°C in 1984 to 28.59°C in 2013, and UHI spatial extent increased from 147.06 km² to 332.36 km². The authors conclude that land use/land cover (LULC) change driven by urbanization is the main driver of UHI amplification in Lagos, and recommend expanding urban vegetation, deploying high-albedo roofing materials, and designing street canyons to improve ventilation, with priority along the Ifako/Ijaye, Oshodi/Isolo, and Lagos Island corridor (Ibeabuchi et al., 2026). Advances in remote sensing have enhanced UHI mapping through LST derived from Landsat thermal bands. LST correlates strongly with LULC because different land covers exhibit distinct thermal, moisture, and radiative properties (Chakraborti et al., 2019; Amiri et al., 2009). Vegetation indices such as NDVI (Normalized Difference Vegetation Index) are inversely related to LST and respond sensitively to land cover transitions (Malik et al., 2019). Modifying LULC composition can mitigate UHI, although anthropogenic factors such as building density and energy consumption are often omitted due to data limitations (Wang et al., 2022). Surface UHI, as defined by Voogt and Oke (2003), examines temporal changes in surface temperature between urban and rural areas. Land cover change further modifies net radiation, which controls partitioning of energy into sensible, latent, and soil heat fluxes (Järvi et al., 2011; Feyisa et al., 2014). Reliable net radiation data are therefore critical for modeling urban energy balance and climate response (Kalthoff et al., 2006; Blonquist et al., 2009).

For Lagos metropolis, this study utilized Landsat data for the three epochs of 1984, 2000, and 2013 to derive NDVI, LST, net radiation, and urban–rural landscape patterns. GIS was employed to analyze spatial variation in temperature, vegetation, and energy fluxes, while Principal Component Analysis (PCA) was applied to identify dominant governing factors and quantify interactions among vegetation, radiative variables, and UHI dynamics. This study addresses a gap in Lagos-specific UHI research by statistically linking urban expansion, LST, and net radiation to UHI using PCA. The findings are also relevant for Lagos State climate adaptation planning, particularly in identifying priority corridors for heat mitigation. The objective is to analyze UHI dynamics in Lagos metropolis from 1984 to 2013, structured into: 1) characterization of climate variables across the three epochs, 2) extraction of dominant factors controlling UHI using PCA, and 3) quantification of UHI temporal dynamics over time.

2. Study Area

Lagos metropolis refers to the continuous built-up zone of Lagos State, Nigeria, including Ojo, Ikotun, Egbe, Agege, Alimosho, Ketu, and Lagos Island. Created in 1967, Lagos served as Nigeria's federal capital until 1991, a period that accelerated its urban growth and infrastructural development. The metropolis covers 1,171 km², with lagoons and waterways accounting for 221 km², forming a complex coastal landscape dominated by the Lagos Lagoon and Atlantic coastline. It lies between 507,933.87 m and 574,309.95 m Easting and 740,347.79 m and 706,462.40 m Northing in UTM Zone 31N (Figure 1). Administratively, Lagos metropolis comprises 16 of the state's 20 Local Government Areas (LGA), housing the core commercial, industrial, and residential districts. It is Nigeria's most densely populated urban area, with 7,937,932 residents in 2006 and 13,491,800 in 2022 (Federal Republic of Nigeria Official Gazette, 2009; World Population Review, n.d.). Lagos experiences a wet equatorial climate with two rainy seasons. Peak rainfall occurs April–July, with monthly averages exceeding 300 mm, while October–November is drier. Heavy rains often cause flooding due to poor drainage in the coastal lowlands (Abegunde, 1987). The harmattan season runs December–February, bringing dry northeasterly winds. Mean temperatures vary from 25 °C in July to 29 °C in March, with January averaging 27 °C (Abegunde, 1987), creating reliably high humidity and thermal stress conditions relevant to urban heat studies.

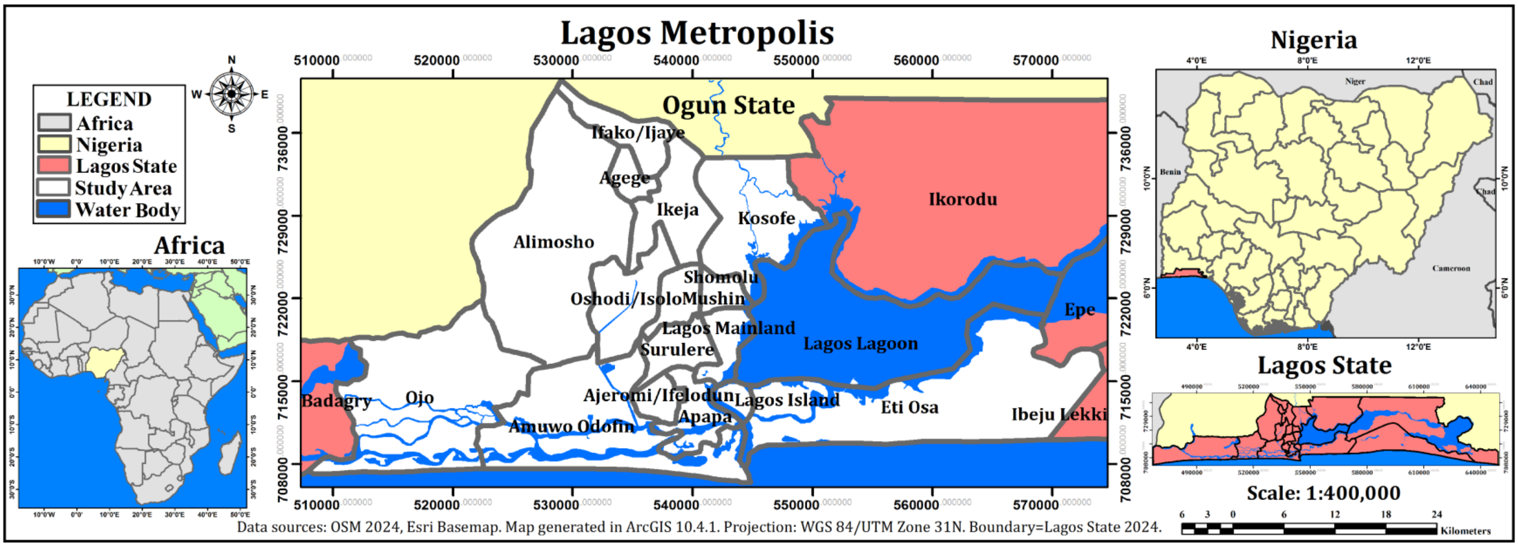

Fig. 1. Lagos Metropolis Administrative Area with Inset Maps of Lagos State, Nigeria and Africa for Details.

3. Methodology

Vegetation and radiative controls on UHIs in the Lagos Metropolis from 1984 to 2013 were assessed using Principal Component Analysis (PCA) of urban built-up fraction, NDVI, LST, and net radiation (Rn). United States Geological Survey (USGS) Landsat Thematic Mapper (TM) 5, Enhanced Thematic Mapper Plus (ETM+) 7, and Operational Land Imager (OLI) 8 imagery provided data for urban-rural differences, LST, Rn, and NDVI for 1984, 2000, and 2013 (Tables 1 and 2). These data were used to evaluate changes in land cover, temperature, vegetation, and energy balance.

For the Lagos metropolis, Landsat Bands 7, 5, and 4 for TM/ETM+ and Bands 7, 6, and 4 for OLI were processed in IDRISI TerrSet 18.31 (Table 2). Images were mosaicked, radiometrically calibrated, and composited to cloud-free scenes for each epoch. A supervised maximum likelihood classifier categorized Land Use/Land Cover (LULC) into built-up area, other land, and water body. Classification accuracy assessment against Google Earth Pro validation data in IBM SPSS Statistics 26 was 80.20% for 1984, 86.40% for 2000, and 86.60% for 2013. The 80.20% accuracy for 1984 implies ±10% uncertainty in UHI boundaries. The urban–rural landscape was mapped in ArcGIS 10.4.1 using the Urban Landscape Analysis Tool (ULAT). Seven classes—urban, suburban, and rural built-up; urban, captured, and rural open land; and water—were delineated, with total area computed using the Calculate Area tool in ArcGIS 10.4.1.

Land Surface Temperature (LST) was retrieved using IDRISI TerrSet 18.31 following USGS protocols (USGS, 2019; Chander & Markham, 2003). Thermal Band 6 for TM, Band 6 High Gain for ETM+, and Band 10 for OLI (Table 2) were converted to top-of-atmosphere (TOA) radiance and brightness temperature using single-channel algorithms for 1984, 2000, and 2013 as follows:

Table 1. GIS Data Acquired for This Research.

Data	Format	Source(s)	Date	Purpose
(1) Landsat imagery TM 5, ETM+ 7, OLI 8	GeoTIFF	USGS Earth Explorer: https://earthexplorer.usgs.gov/	18/12/1984, 06/02/2000, 25/03/2013	LULC, LST, NDVI, Rn
(2) Administrative map of Lagos State	Shapefile	Guinea Current Large Marine Ecosystem and UNILAG Regional Centre for Environmental Management	2010	Study area boundary
(3) High-resolution imagery, Google Earth Pro 7.3 edition	JPEG	Google Earth: https://www.google.com/earth/about/versions/	2017	Accuracy assessment
(4) GPS points from ground-truthing	CSV/Shapefile	Field survey using Garmin GPS	2020	Accuracy assessment, Validation

Note. LULC = Land Use/Land Cover; LST = Land Surface Temperature; Rn = Net Radiation; NDVI = Normalized Difference Vegetation Index; TM = Thematic Mapper; ETM+ = Enhanced Thematic Mapper Plus; OLI = Operational Land Imager; UNILAG = University of Lagos.

Table 2. Landsat Thematic Mapper 5, Enhanced Thematic Mapper Plus 7, and Operational Land Imager 8 Sensor Characteristics.

Sensor	Path/Row	Spectral Range (µm)	Bands	Spatial Resolution (m)	Acquisition Time	Acquisition Date
TM 5- Multispectral	191/055,056	0.45–2.35	3, 4, 5, 7	30	09:33	18/12/1984
TM 5- TIRS	191/055,056	10.40–12.50	6	120	09:33	18/12/1984
ETM+ 7- Multispectral	191/055,056	0.45–2.35	3, 4, 5, 7	30	09:56	06/02/2000
ETM+ 7-TIRS	191/055,056	10.40–12.50	6H	60	09:56	06/02/2000
OLI 8- Multispectral	191/055,056	0.53–2.29	3, 4, 5, 7	30	10:04	25/03/2013
OLI 8-TIRS	191/055,056	10.60–12.51	10	100	10:04	25/03/2013

Note. H = high gain; TIRS = Thermal Infrared Sensor; TM = Thematic Mapper; ETM+ = Enhanced Thematic Mapper Plus; OLI = Operational Land Imager

TOA spectral radiance:

$$L_\lambda = \left(\frac{LMAX_\lambda - LMIN_\lambda}{QCALMAX - QCALMIN}\right) \times (QCAL - QCALMIN) + LMIN_\lambda \quad (1)$$

$$T_b = \frac{K_2}{\ln[(K_1 / L_\lambda) + 1]} \quad (2)$$

Where L_λ= Spectral radiance [W/(m^2·sr·µm)]; Q_{CAL} = Quantized calibrated pixel value (DN for thermal band); $LMIN_\lambda/LMAX_\lambda$ = Spectral radiance scaling factors for the thermal band from image metadata; $QCAL_{MIN}/QCAL_{MAX}$ = 1 and 255 respectively; T_b = At-sensor brightness temperature (Kelvin); K_1 and K_2 = Thermal conversion constants specific to each band [W/(m^2·sr·µm) and Kelvin] for Landsat TM Band 6, ETM+ Band 6, and OLI Band 10.

Surface emissivity:

$$\varepsilon = \varepsilon_v P_v + \varepsilon_s (1 - P_v) + C \quad (3)$$

$$P_v = 1 - \left(\frac{NDVI - NDVI_{MIN}}{NDVI_{MAX} - NDVI_{MIN}}\right)^2 \quad (4)$$

Where ε = Surface emissivity; ε_v and ε_s = Vegetation and soil emissivity; P_v = Vegetation proportion; C = Surface roughness (Snyder et al., 1998); NDVI = Normalized Difference Vegetation Index; $NDVI_{MAX}$ = Maximum NDVI value in the image; $NDVI_{MIN}$ = Minimum NDVI value in the image.

Land surface temperature conversion:

$$T_{LST}(K) = \frac{T_b}{1 + (\lambda \times T_b / \rho) \ln \varepsilon} \quad (5)$$

Where $T_{LST}(K)$ = Land Surface Temperature in Kelvin; T_b = At-sensor brightness temperature in Kelvin; λ = Wavelength of emitted radiance (µm). λ = 11.5 µm for Landsat 5 TM Band 6 and Landsat 7 ETM+ Band 6, and λ = 10.9 µm for Landsat 8 OLI Band 10; ε = Surface emissivity and ρ = h×c/σ = 1.438 × 10^{-2} m·K.

Temperature conversion, degrees Celsius:

$$T_{LST}(°C) = T_{LST}(K) - 273.15 \quad (6)$$

Where $T_{LST}(K)$ = Land Surface Temperature in degrees Celsius; $T_{LST}(K)$ = Land Surface Temperature in Kelvin.

Net radiation was calculated in IDRISI TerrSet 18.31 following Parlow (1998) and Monteith and Unsworth (2013):

$$Rn = (1 - \alpha)\, Rsin + \varepsilon_a \sigma T_a^4 (1 + 0.17N^2) - \varepsilon_s \sigma T_s^4 \quad (7)$$

Where α = Surface albedo, Rsin = Incoming shortwave radiation (W/m²), ε_a and ε_s = Air and surface emissivity, σ = Stefan–Boltzmann constant (5.67 × 10^{-8} W/m²·K^{-4}), T_a and T_s = Air and surface temperature (K), and N = Cloud fraction.

NDVI in IDRISI TerrSet 18.31 was calculated as (NIR - R) / (NIR + R) (Rouse et al., 1973), using Bands 4 and 3 for Landsat TM 5/ETM+ 7 and Bands 5 and 4 for Landsat OLI 8, where NIR denotes near-infrared and R denotes red (Table 2).

Dimensionality reduction was done using PCA in IBM SPSS Statistics 26 on standardized variables: urban built-up area, LST, NDVI, and Rn. UHI and non-UHI zones were delineated using the mean urban LST threshold for each epoch (Ibeabuchi et al., 2026; Voogt & Oke, 2003; Weng & Fu, 2014). UHI areal extent was computed in ArcGIS 10.4.1 using the Calculate Areas tool.

Pearson correlation assessed relationships among UHI area, built-up area, and LST. With only three observations (N = 3), results are exploratory and indicate trend-level patterns rather than statistical significance. The coefficient was calculated as:

$$r = \frac{N(\sum XY) - (\sum X \sum Y)}{\sqrt{\left[N\sum X^2 - (\sum X)^2\right]\left[N\sum Y^2 (\sum Y)^2\right]}} \quad (8)$$

Where r = Correlation coefficient; N = Total number of samples; X = Independent variable; Y = Dependent variable; Σ = Summation function. Descriptive statistics (minimum, maximum and mean) were computed in Microsoft Excel 2010, and maps were produced in ArcGIS 10.4.1.

4. Results

4.1 Dynamic Factors of the Urban Climate for 1984, 2000 and 2013

Urban-rural landscape maps for 1984, 2000, and 2013 are shown in Figure 2. Urban built-up area increased from 242.41 km² in 1984 to 563.28 km² in 2013, while rural open land declined from 354.74 km² to 115.19 km². Table 3 presents area statistics. LST maps are shown in Figure 2. Mean LST in urban built-up areas rose from 24.76°C in 1984 to 28.59°C in 2013. Table 3 provides descriptive statistics. Net radiation maps are shown in Figure 2. Urban areas exhibited higher net radiation than rural areas across all years. Table 3 provides values. NDVI maps are shown in Figure 2. Mean NDVI declined in urban areas, reflecting vegetation loss. Table 3 provides statistics.

4.2 Factor Structure Underlying Urban Climate in Lagos

A Principal Component Analysis was conducted on four environmental variables—Urban Built-up Area, Land Surface Temperature, Net Radiation, and the Normalized Difference Vegetation Index—to identify the dominant modes of urban climate variability in Lagos. The correlation matrix indicated strong interdependence among the variables, with Land Surface Temperature and Net Radiation exhibiting a correlation coefficient of 0.998 (Table 4). The determinant of the matrix approached zero, confirming high multicollinearity and supporting the use of PCA for dimensionality reduction.

4.2.1 Component Extraction and Variance Explained

Kaiser's eigenvalue-greater-than-one criterion was applied to determine the number of retained components (Kaiser, 1960). Two principal components were retained from the four input variables. Component 1 exhibited an eigenvalue of 2.716 and explained 67.89% of total variance. Component 2 yielded an eigenvalue of 1.284 and accounted for 32.11% of variance. Collectively, the two-component solution explained 100% of variance in the original dataset. Components 3 and 4, with eigenvalues < 1.0, were excluded as they contributed negligible explanatory power. The cumulative variance of 100% indicates complete representation of dataset variability by the reduced factor space (Table 5).

4.2.2 Rotated Factor Loadings and Interpretation

A varimax rotation with Kaiser normalization converged after three iterations, producing an orthogonal solution with interpretable loadings (Table 6). A loading threshold of < 0.90 was applied to define variable membership within each factor. Component 1 displayed strong positive loadings for LST, Net Radiation, and Urban Built-up Area. This pattern reflects the coupled influence of urban expansion on surface temperature and the surface radiation budget. Accordingly, Component 1 was named the Urban Thermal-Radiative Factor. Component 2 loaded almost exclusively on the NDVI, with a minor secondary loading on Urban Built-up Area. This factor represents the moderating effect of vegetation on surface energy exchange and was designated the Vegetation Factor.

4.2.3 Model Adequacy and Variable Relationships

The two-factor solution reproduced the observed correlations with all reproduced residuals below 0.05, indicating an acceptable fit (Table 7). Urban Built-up Area exhibited moderate loadings on both factors, suggesting its dual role in driving thermal change and in replacing vegetated land cover.

4.2.4 Summary of Factor Analysis

Dimensionality reduction condensed the four original variables into two independent factors that fully account for the observed variance (Table 8 and 9). The "Urban Thermal-Radiative Factor" and the "Vegetation Factor" constitute the primary statistical controls on urban climate variability in Lagos. The cross-loading of Urban Built-up Area underscores its function both as a source of surface warming and as a proxy for vegetation loss.

4.3 Dynamics of Urban Heat Island

Surface UHI zones were mapped using epoch-specific LST thresholds based on mean urban built-up temperatures: 24.76°C for 1984, 27.99°C for 2000, and 28.59°C for 2013 (Figure 3; Ibeabuchi et al., 2026; Weng & Fu, 2014). UHI area expanded from 125.01 km² in 1984 to 166.01 km² in 2000 and 319.38 km² in 2013 (Table 10). Non-UHI area declined from 866.96 km² to 825.96 km² and 672.59 km² over the same period (Table 10), reflecting outward spread of elevated temperatures into cooler peripheries. This 155.4% increase in UHI extent aligns with intensification trends in rapidly urbanizing African cities (Ojeh et al., 2016; Estoque et al., 2017). Thermal profiles of UHI versus non-UHI zones are shown in Table 11. Mean LST in UHI zones rose from 25.41°C to 29.96°C, while non-UHI zones increased from 22.72°C to 25.09°C. The thermal differential thus widened from 2.69°C to 4.87°C, indicating stronger UHI intensity over time. Spatially, thermal anomalies were initially limited to the central business district in 1984 but expanded by 2013 to Alimosho, Ifako Ijaye, Kosofe, Ojo, Amuwo Odofin, and Eti Osa (Figure 3). These districts are marked by dense development and low vegetation cover (Ibeabuchi & Oni, 2013; Amiri et al., 2009), consistent with the inverse NDVI-LST relationship observed in tropical cities. Pearson correlation analysis examined linkages among UHI area, built-up area, and mean LST (Table 12). With $n=3$, results are exploratory and indicate trends rather than statistical inference. UHI area correlated strongly with built-up area ($r = 0.99$, $p = 0.03$), confirming urban expansion as a key driver of UHI growth (Estoque et al., 2017). Positive but non-significant correlations were found between UHI area and mean LST ($r = 0.77$, $p = 0.45$) and between built-up area and mean LST ($r = 0.74$, $p = 0.47$), supporting the thermal influence of impervious surfaces (Weng et al., 2001).

5. Discussion

Between 1984 and 2013, Lagos experienced extensive land use and land cover conversion associated with rapid urbanization, a pattern documented in other fast-growing tropical cities (Estoque et al., 2017; He et al., 2021). Built-up surfaces expanded by 56.78%, while rural open areas contracted by 11.61% (Table 3). The replacement of vegetation with impermeable surfaces reduced evapotranspiration and shade, altered the surface energy balance, and increased the urban-rural temperature contrast. This mechanism is consistent with surface energy balance theory of Urban Heat Island development (Oke, 1982; Arnfield, 2003). Spatial-temporal analysis showed consistent thermal contrasts among land cover classes. Rural open areas had lower land surface temperature than urbanized and encroached open areas in all three periods (Table 3), supporting evidence that vegetation mitigates surface warming (Amiri et al., 2009; Chakraborti et al., 2019). Higher temperatures in urban zones reflect the dominance of impermeable materials with high heat capacity and low albedo, which absorb solar radiation and release it as sensible heat (Aflaki et al., 2017).

The PCA of urban built-up area, LST, net radiation, and NDVI produced two orthogonal factors that explained 100% of the variance in the four input variables. The correlation matrix (Table 3) exhibited near-singularity (determinant ≈ 0.000; LST-Net Radiation correlation = 0.998). High collinearity between LST and net radiation was retained because both variables represent distinct components of the surface energy balance.

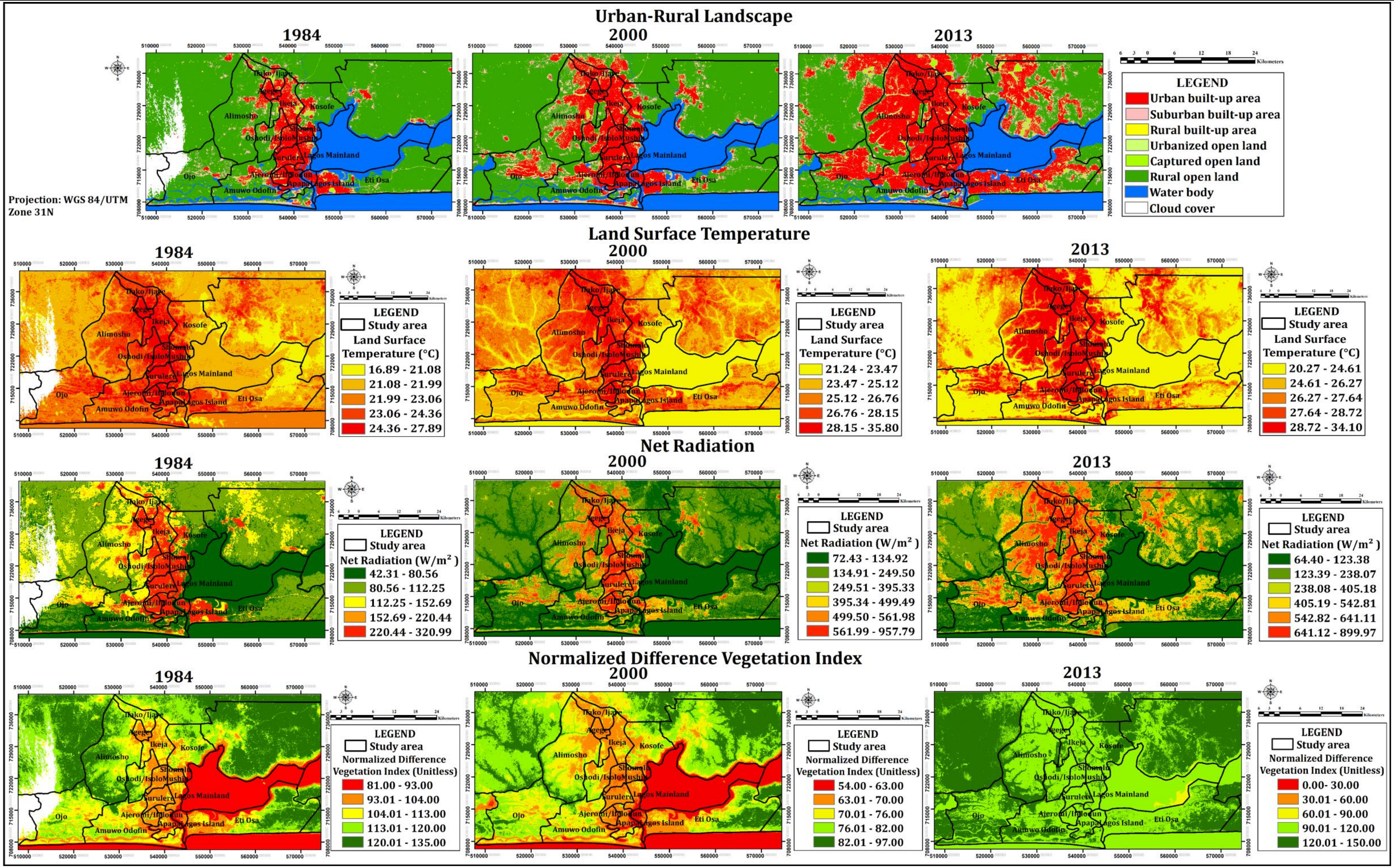

Fig. 2. Spatiotemporal Patterns of Urban-Rural Landscape, Land Surface Temperature, Net Radiation, and Normalized Difference Vegetation Index in Lagos Metropolis, 1984, 2000, and 2013.
Note. Urban-rural map: IDRISI TerrSet 18.31, ArcGIS 10.4.1. LST: single-channel algorithm. NDVI: (NIR-Red)/(NIR+Red), scaled 0-255. Net radiation: shortwave + longwave. Source: Landsat TM/ETM+/OLI.

Table 3. Urban-Rural Landscape Category Area and Land Surface Temperature, Net Radiation, And Normalized Difference Vegetation Index Statistics for Lagos Metropolis, 1984–2013.

	Urban-Rural Landscape Area (km²)			**Land Surface Temperature** (°C)		
				1984	**2000**	**2013**
Category	**1984**	**2000**	**2013**	**Min/Max/Mean**	**Min/Max/Mean**	**Min/Max/Mean**
No Data	24.14	0.00	0.00	0.00/0.00/0.00	0.00/0.00/0.00	0.00/0.00/0.00
Urban built-up	242.41	296.46	563.28	20.20/27.90/24.76	22.67/35.80/27.99	21.46/33.60/28.59
Suburban built-up	68.14	69.37	58.74	19.30/27.30/23.61	22.39/31.13/27.08	20.79/32.61/25.37
Rural built-up	8.14	4.95	3.31	20.20/26.80/22.93	22.10/30.07/26.91	20.79/26.77/23.15
Urbanized openland	169.07	158.04	151.74	18.60/27.10/23.43	22.10/32.71/26.66	20.70/32.48/25.24
Captured openland	13.64	12.62	14.31	19.70/26.80/23.07	23.23/30.60/25.87	20.70/30.14/24.20
Rural openland	354.74	352.03	115.19	17.90/26.80/22.02	22.10/30.87/24.67	20.63/30.33/23.32
Water body	111.54	98.34	85.26	18.80/25.50/22.16	21.25/27.38/22.91	20.78/29.27/22.33

	Net Radiation (W/m²)			**Normalized Difference Vegetation Index**		
	1984	**2000**	**2013**	**1984**	**2000**	**2013**
Category	**Min/Max/Mean**	**Min/Max/Mean**	**Min/Max/Mean**	**Min/Max/Mean**	**Min/Max/Mean**	**Min/Max/Mean**
No Data	0.00/0.00/0.00	0.00/0.00/0.00	0.00/0.00/0.00	0.00/0.00/0.00	0.00/0.00/0.00	0.00/0.00/0.00
Urban built-up	57.50/320.99/254.40	85.32/957.80/517.67	79.83/868.28/590.75	60.71/145.61/99.54	58.67/81.77/67.93	93.60/143.24/111.90
Suburban built-up	45.68/308.91/163.86	80.44/686.65/286.73	72.01/667.16/299.82	57.69/153.72/115.48	57.14/82.42/71.37	90.33/143.20/117.81
Rural built-up	49.13/206.01/131.23	87.18/414.48/204.30	75.12/300.85/186.14	65.38/158.88/122.68	57.14/83.83/74.33	93.57/139.36/118.08
Urbanized openland	57.10/299.04/169.55	84.85/753.22/310.92	79.28/750.80/199.09	57.14/163.27/121.46	60.13/86.03/73.48	93.01/145.58/124.56
Captured openland	53.28/291.27/144.29	89.50/622.67/258.99	76.13/638.32/159.72	73.53/150.91/125.26	65.41/86.49/75.20	107.37/145.46/130.19
Rural openland	42.32/279.82/99.27	72.43/609.39/145.14	66.23/469.69/108.47	60.00/173.33/139.99	59.46/91.43/78.99	95.18/147.83/131.32
Water body	48.35/291.27/68.97	72.43/602.19/100.98	64.40/587.13/89.61	37.21/154.78/88.31	55.56/80.00/63.27	89.51/138.35/97.61

Notes. 1. NDVI is unitless, range -1 to +1. Table values scaled to 0-255 for visualization. 2. Min/Max/Mean = minimum/maximum/mean for each zone. 3.No Data pixels = cloud/cloud shadow and were excluded from statistical analysis.

Factor 1, the "Urban Thermal-Radiative Factor," accounted for 67.89% of variance and had loadings of 0.999 for LST, 1.000 for net radiation, and 0.764 for urban built-up area (Table 8). It captures the combined influence of urban expansion on LST and the radiation budget. The strong loading of net radiation indicates reduced outgoing longwave radiation and increased sensible heat flux over built-up surfaces, directly linking the factor to surface energy balance processes. This is consistent with the observed UHI intensification in Lagos. Factor 2, the "Vegetation Factor," accounted for 32.11% of variance and loaded 0.998 on NDVI, illustrating the cooling and moisture-regulating role of vegetation (Table 8). Urban built-up area loaded on both factors, indicating its dual role as a driver of thermal change and a proxy for vegetation loss. Model adequacy was confirmed by reproduced residuals below 0.05 for all variable pairs (Table 7).

Table 4. Correlation (r) Matrix.

Variable	UBA	LST	Rn	NDVI
UBA	1.000	0.736	0.777	0.599
LST	0.736	1.000	0.998	-0.101
Rn	0.777	0.998	1.000	-0.040
NDVI	0.599	-0.101	-0.040	1.000

Note. $p < 0.01$, $n = 3$. Determinant = 0.000. This matrix is not positive definite. LST–Rn r= 0.998 indicates multicollinearity. UBA= Urban Built-up Area, LST= Land Surface Temperature, Rn= Net Radiation, NDVI = Normalized Difference Vegetation Index.

Table 5. Total Variance Explained.

	Initial Eigen Values		
Component	**Total**	**% of Variance**	**Cumulative %**
1	2.716	67.888	67.888
2	1.284	32.112	100.000
3	0.00	0.00	100.000
4	0.00	0.00	100.000
	Sums of Squared Loadings		
Component	**Total**	**% of Variance**	**Cumulative %**
1	2.716	67.888	67.888
2	1.284	32.112	100.000
3			
4			

Note. Extraction Method: PCA. Components with eigenvalues greater than 1 were retained per Kaiser criterion. Extraction sums of squared loadings account for 100% of total variance. Results indicate two dominant factors representing the underlying structure of the dataset.

Table 6. Component Matrix.

	Component	
Variable	**1**	**2**
UBA	0.923	0.384
LST	0.940	-0.341
Rn	0.959	-0.283
NDVI	0.244	0.970

Note. Extraction Method: PCA. Two components extracted. UBA= Urban Built-up Area, LST= Land Surface Temperature, Rn= Net Radiation, NDVI= Normalized Difference Vegetation Index.

Table 7. Reproduced Correlations[a,b].

	Reproduced Correlations			
Variable	UBA	LST	Rn	NDVI
UBA	1.000[a]	0.736	0.777	0.599
LST	0.736	1.000[a]	0.998	-0.101
Rn	0.777	0.998	1.000[a]	-0.040
NDVI	0.599	-0.101	-0.040	1.000[a]
	Residual[b]			
Variable	UBA	LST	Rn	NDVI
UBA		-0.00	-0.00	0.00
LST	-0.00		-0.00	0.00
Rn	-0.00	-0.00		0.00
NDVI	0.00	0.00	0.00	

Note. Extraction Method: PCA. a= Reproduced communalities. b =No residuals >0.05. UBA= Urban Built-up Area, LST= Land Surface Temperature, Rn= Net Radiation, NDVI= Normalized Difference Vegetation Index.

Table 8. Rotated Component Matrix.

Variable	**1**	**2**
UBA	0.764	0.645
LST	0.999	-0.042
Rn	1.000	0.020
NDVI	-0.060	0.998

Note. Extraction Method: PCA. Rotation Method: Varimax with Kaiser normalization. UBA= Urban Built-up Area, LST= Land Surface Temperature, Rn= Net Radiation, NDVI= Normalized Difference Vegetation Index.

Table 9. Component Transformation Matrix.

Component	1	2
1	0.953	0.302
2	-0.302	0.953

Note. Extraction Method: PCA. Rotation Method: Varimax with Kaiser normalization.

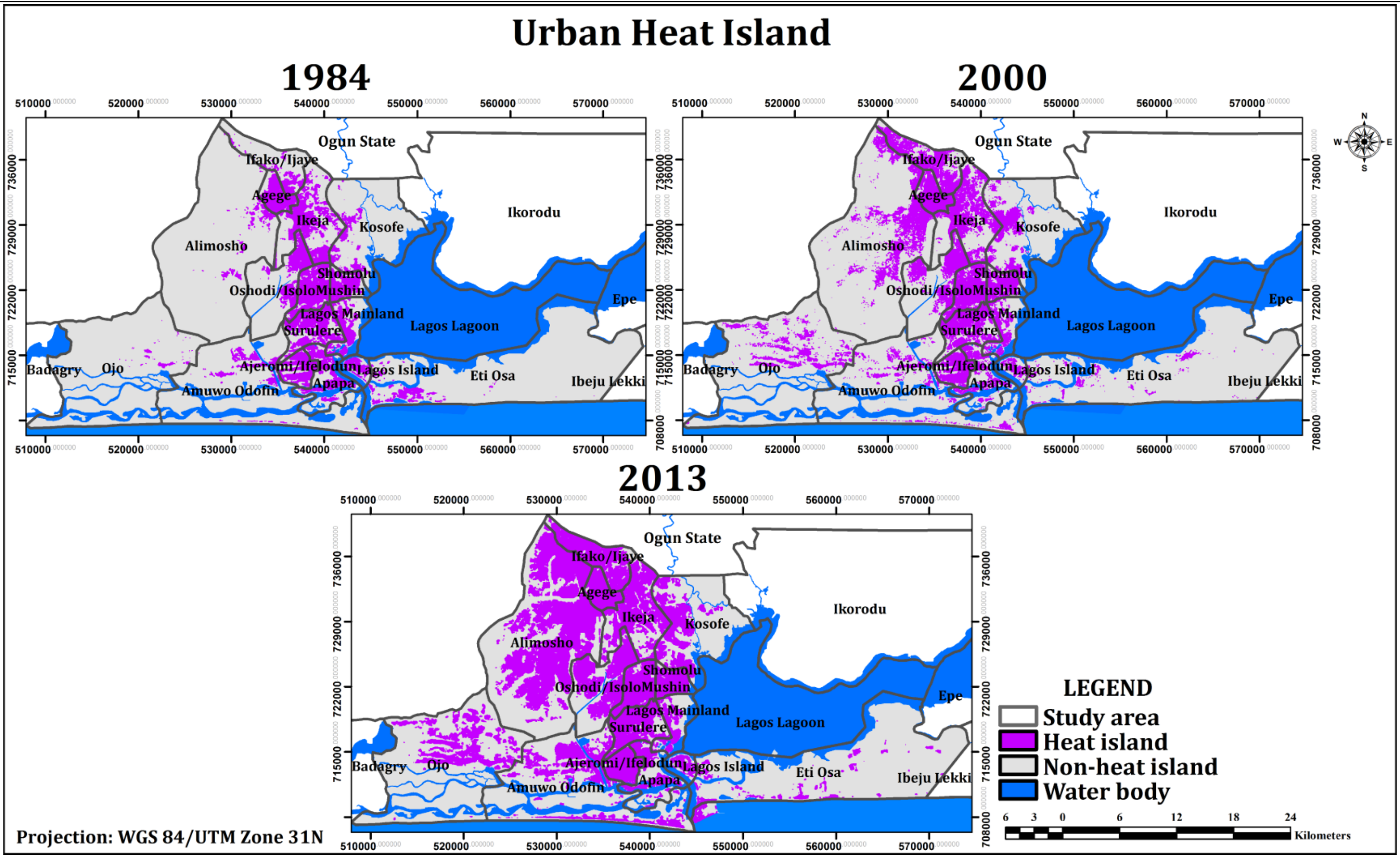

Fig. 3. Spatio-Temporal Distribution of Surface Urban Heat Island (UHI) in Lagos Metropolis, 1984–2024.
Note. UHI zones derived using epoch-specific mean LST thresholds for urban built-up pixels from Landsat thermal bands.

.**Table 10**. Areal Extent of UHI and Non-UHI Zones in Lagos Metropolis, 1984–2013.

	Spatial Extent (km²)	
Year	**Non-UHI**	**UHI**
1984	866.96	125.01
2000	825.96	166.01
2013	672.59	319.38

Note. UHI = Urban Heat Island zone. Non-UHI = Non-Urban Heat Island area below the epoch-specific UHI threshold.

Land cover change also modified the radiation budget. Peak net radiation occurred in the urban core and in Ifako/Ijaye, Eti Osa, Alimosho, and Ojo LGAs, where surfaces with high LST received the greatest radiative input (Figure 2). This result aligns with studies showing that urban materials enhance net radiation and heat retention (Golden & Kaloush, 2006; Grimmond, 2006). The inverse relationship between NDVI and LST loadings (Table 4) further supports the conclusion that vegetation loss intensifies surface warming (Malik et al., 2019; Xian, 2021).

Table 11. Summary of Land Surface Temperature Statistics for UHI and Non-UHI Zones, 1984–2013 (°C).

	1984	2000
Catergory	**Min/Max/Mean**	**Min/Max/Mean**
Non-UHI	17.90/27.70/22.72	21.25/31.13/25.45
UHI	23.60/27.90/25.41	28.19/35.80/28.71
	2013	
Catergory	**Min/Max/Mean**	
Non-UHI	20.63/32.61/25.09	
UHI	28.59/33.60/29.96	

Note. Min/Max/Mean = Minimum/Maximum/Mean LST in °C. UHI = Urban Heat Island. Non-UHI = Non-Urban Heat Island.

Table 12. Pearson Correlations Among UHI Area, Built-Up Area, and Mean LST, 1984–2013.

Variable		UHIA	BUA	LST
UHIA	Pearson Correlation (r)	1.00	0.99*	0.77
	Significant (2-tailed)	0.00	0.03	0.45
	N	3	3	3
BUA	Pearson Correlation	0.99*	1.00	0.74
	Significant (2-tailed)	0.03	0.00	0.47
	N	3	3	3
LST	Pearson Correlation	0.77	0.74	1.00
	Significant (2-tailed)	0.45	0.47	0.00
	N	3	3	3

Note. *$p < 0.05$, two tailed. N = 3 years. BUA = Built-up Area, LST = Land Surface Temperature, UHIA = Urban Heat Island Area.

The intensification of the Urban Heat Island has implications for human health and energy demand. The 4.87°C urban-rural temperature difference recorded in 2013 approaches thresholds linked to increased heat-related mortality in tropical regions. Elevated temperatures increase heat stress for vulnerable populations and raise cooling energy demand (Coumou &

Rahmstorf, 2012; Rajagopalan et al., 2014). Higher near-surface temperatures can also suppress vertical mixing, reducing pollutant dispersion and degrading air quality (Baklanov et al., 2016). Key limitations include reliance on three time slices, which limits temporal resolution and statistical power for trend detection. Classification accuracies of 80.2%–86.6% introduce uncertainty, particularly for mixed pixels at the urban-rural fringe in 1984. Future studies should incorporate direct estimates of sensible heat flux, latent heat flux, and ground heat storage, and use annual Landsat composites to improve trend analysis (Järvi et al., 2011; Hou et al., 2019). Overall, UHI expansion in Lagos coincided with growth in built-up area and rising LST from 1984 to 2013. PCA indicates that processes linked to urbanization and vegetation cover are the primary statistical controls on the city's urban climate.

6. Conclusion and Recommendations

6.1 Conclusion

Analysis of Landsat imagery for 1984, 2000, and 2013 shows that Urban Heat Island extent, built-up area, and land surface temperature in Lagos increased concurrently. PCA reduced the multivariate drivers to two factors: an "Urban Thermal-Radiative" factor and a "Vegetation" factor. The 4.87°C urban-rural land surface temperature difference in 2013 approaches thresholds associated with elevated heat mortality risk in tropical cities. Continued replacement of vegetation and open land with impermeable surfaces is expected to intensify thermal stress.

6.2 Policy Brief for Lagos State Physical Planning Authority

6.2.1 Urban Heat Island Mitigation Priorities for Lagos Metropolis

Issue: Continuous growth in built-up area and land surface temperature since 1984 has broadened Urban Heat Island coverage and increased heat exposure.

Main Finding: The "Urban Thermal-Radiative" factor, defined by urban built-up area, land surface temperature, and net radiation, is the dominant statistical driver of Lagos's urban climate, while vegetation cover provides a counteracting effect.

Priority LGAs for Intervention:

Tier 1 – Urgent: Alimosho, Eti Osa, Ifako-Ijaiye, Ojo
Tier 2 – High Priority: Amuwo-Odofin, Mushin, Agege, Kosofe
Tier 3 – Monitor: Surulere, Lagos Mainland, Ajeromi-Ifelodun, Apapa
Tier 4 – Maintain: Lagos Island, Ikeja, Shomolu, Oshodi-Isolo

Proposed Measures

1. Expand green infrastructure: Require ≥ 15% green space in new developments and retrofit 5% of public open areas in Tier 1 LGAs by 2027.

2. Adopt high-reflectivity materials: Pilot reflective roofing and cool pavement in Tier 1 commercial zones through public procurement.

3. Integrate Urban Heat Island assessment into planning: Mandate quantitative Urban Heat Island impact assessments for developments > 5,000 m² in Tier 1 and 2 LGAs, using urban built-up area and NDVI as screening indicators consistent with factor loadings.

Next Actions: Reassess priorities using satellite data from 2020–2024 and conduct field validation in Alimosho and Eti Osa.

6.3 Directions for Future Work

Changes in surface energy partitioning in urban areas alter near-surface temperature through modifications to albedo, surface roughness, and soil moisture. This study characterized the Urban Heat Island using land surface temperature, land use and land cover, NDVI, and net radiation but did not quantify sensible heat flux, latent heat flux, or ground heat storage. Future research should combine satellite-derived land surface temperature with surface energy balance modeling to clarify the physical mechanisms underlying the "Urban Thermal-Radiative" factor identified here. This will move beyond correlative analysis to mechanistic explanation of heat flux dynamics in Lagos.

Reference

1. Abegunde, M.A.A. (1987). Aspects of the physical environment of Lagos. In A. Adefuye, A. Babatunde, J. Osuntokun (Eds.), History of the people of Lagos State (pp. 6-11). Lantern Books.

2. Aflaki, A., Mirnezhad, M., Ghaffarianhoseini, A., Ghaffarianhoseini, A., Omramy, H., Wang, Z, -H., & Akbari, H. (2017). Urban heat island mitigation strategies: A state-of-the-art review on Kuala Lumpur, Singapore and Hong Kong. Cities, 62, 131–145. https://doi.org/10.1016/j.cities.2016.09.003

3. Amiri, R., Weng, Q., Alimohammadi, A., & Alavipanah, S.K. (2009). Spatial–temporal dynamics of land surface temperature in relation to fractional vegetation cover and land use/cover in the Tabriz urban area, Iran. Remote Sensing of Environment, 113(12), 2606–2617. https://doi.org/10.1016/j.rse.2009.07.021

4. Arnfield, A.J. (2003). Two decades of urban climate research: A review of turbulence, exchanges of energy and water, and the urban heat island. International Journal of Climatology, 23(1), 1−26. https://doi.org/10.1002/joc.859

5. Athukorala, D., & Murayama, Y. (2021). Urban heat island formation in greater Cairo: Spatio-temporal analysis of daytime and nighttime land surface temperatures along the urban–rural gradient. Remote Sensing, 13(7),1396. https://doi.org/10.3390/rs13071396

6. Baklanov, A., Molina, L.T., & Gauss, M. (2016). Megacities, air quality and climate. Atmospheric Environment, 126, 235–249. https://doi.org/10.1016/j.atmosenv.2015.11.059

7. Blonquist, J.M., Jr., Tanner, B.D., & Bugbee, B. (2009). Evaluation of measurement accuracy and comparison of two new and three traditional net radiometers. Agricultural and Forest Meteorology, 149(10), 1709–1721. https://doi.org/10.1016/j.agrformet.2009.05.015

8. Chander, G., & Markham, B. (2003). Revised Landsat-5 TM radiometric calibration procedures and postcalibration dynamic ranges. IEEE Transactions on Geoscience and Remote Sensing, 41(11), 2674- 2677.

9. Chakraborti, S., Banerjee, A., Sannigrahi, S., Pramanik, S., Maiti, A., & Jha, S. (2019). Assessing the dynamic relationship among land use pattern and land surface temperature: A spatial regression approach. Asian Geographer, 36(2), 93–116. https://doi.org/10.1080/10225706.2019.1623054

10. Coumou, D., & Rahmstorf, S.A. (2012). A decade of weather extremes. Nature Climate Change, 2, 491–496. https://doi.org/10.1038/nclimate1452

11. Estoque, R.C., Murayama, Y., & Myint, S.W. (2017). Effects of landscape composition and pattern on land surface temperature: An urban heat island study in the megacities of Southeast Asia. Science of the Total Environment, 577, 349–359. https://doi.org/10.1016/j.scitotenv.2016.10.195

12. Federal Republic of Nigeria Official Gazette. (2009). Legal notice on publication of 2006 census final results (FGP16 /22009 /10,000 (OL02). https://gazettes.africa/archive/ng/2009/ng-government-gazette-dated-2009-02-02-no-2.pdf

13. Feyisa, G. L., Dons, K. & H. Meilby (2014). Efficiency of parks in mitigating urban heat island effect: An example from Addis Ababa. Landscape and Urban Planning, 123, 87–95. https://doi.org/10.1016/j.landurbplan.2013.12.008

14. Gartland, L., & Gonçalves, S.H. (2010). Ilhas de calor: Como mitigar zonas de calor em áreas urbanas. Oficina de Textos.

15. Golden, J.S. & Kaloush, K.E. (2006). Mesoscale and microscale evaluation of surface pavement impacts on the urban heat island effects. The International Journal of Engineerig, 7(1), 37-52. https://doi.org/10.1080/10298430500505325

16. Grimmond, C.S.B. (2006). Progress in measuring and observing the urban atmosphere. Theoretical and Applied Climatology, 84(1-3), 3–22. https://doi.org/10.1007/s00704-005-0140-5

17. He, B-J., Zhao, D., Xiong, K., Qi, J., Ulpiani, G., Pignatta, G., Prasad, D., & Jones, P. (2021). Framework for addressing urban heat challenges and associated adaptive behavior by the public and the issue of willingness to pay for heat resilient infrastructure in Chongqing, China. Sustainable Cities and Society, 75. https://doi.org/10.1016/j.scs.2021.103361

18. Hou, H., Wang, R., & Murayama, Y. (2019). Scenario-based modelling for urban sustainability focusing on changes in cropland under rapid urbanization: A case study of Hangzhou from 1990 to 2035. Science of the Total Environment, 661, 422–431. https://doi.org/10.1016/j.scitotenv.2019.01.208

19. Ibeabuchi, U., Oni, F.O., & Adeaga, O.A. (2026). Dynamics of the Urban Heat Island in Lagos Metropolis, Nigeria (1984 to 2013). IRGS Journal of Multidisciplinary Research and Studies (IRGSJMRS), 1(1), 1–6.

20. Ibeabuchi, U., & Oni, F. (2013). An assessment of urban heat islands within Abeokuta area, South-western Nigeria. Lagos Journal of Geographic Issues, 1(1), 25-42.

21. Järvi, L., Grimmond, C.S.B., & A. Christen (2011). The Surface Urban Energy and Water Balance Scheme (SUEWS): Evaluation in Los Angeles and Vancouver. Journal of Hydrology, 411(3-4), 219–237. https://doi.org/10.1016/j.jhydrol.2011.10.001

22. Kaiser, H.F. (1960). The application of electronic computers to factor analysis. Educational and Psychological Measurement, 20(1), 141–151. https://doi.org/10.1177/001316446002000116

23. Kalthoff,N., Fiebig-Wittmaack,M., Meißner, C., Kohler, M., Uriarte, M., Bischoff-Gauß, I., & Gonzalez, E. (2006). The energy balance, evapo-transpiration and nocturnal dew deposition of an arid valley in the Andes. Journal of Arid Environments, 65(3), 420–443.

24. Malik, M.S., Shukla, J.P., & Mishra, S. (2019). Relationship of LST, NDBI, and NDVI using Landsat-8 data in Kandaihimmat watershed, Hoshangabad, India. Indian Journal of Geo-Marine Sciences, 48 (01), 25-31. https://nopr.niscpr.res.in/handle/123456789/45657

25. Mohajerani, A., Jason Bakaric, J., & Jeffrey-Bailey, T. (2017). The Urban heat island effect, its causes, and mitigation, with reference to the thermal properties of asphalt concrete. Journal of Environmental Management,197, 522–538. https://doi.org/10.1016/j.jenvman.2017.03.095

26. Monteith, J.I., & Unsworth, M.H. (2013). Principles of environmental physics: Plants, animals, and the atmosphere (4th ed.). Academic Press.

27. Ojeh, V.N., Balogun, A.A., & Okhimamhe, A.A. (2016). Urban-rural temperature differences in Lagos. Climate, 4(2),29. https://doi.org/10.3390/cli4020029

Oke, T.R. (1982). The energetic basis of the urban heat island. Quarterly Journal of the Royal Meteorological Society, 108(455), 1-24. https://doi.org/10.1002/qj.49710845502

28. Oke, T.R., Mills, G., Christen, A., & Voogt, J.A. (2017). Urban climates. Cambridge University Press.

29. Parlow, E. (1996). Determination and inter comparison of radiation fluxes and net radiation using Landsat TM data of Liefderjorden/NW-Spitsbergen. In T.-D. Guyenne, Proceedings of the 4th Circumpolar Symposium (pp. 27-32). European Space Agency.

30. Rajagopalan, P., Lim, K.C., & Jamei, E. (2014). Urban heat island and wind flow characteristics of a tropical city. Solar Energy, 107,159–170. https://doi.org/10.1016/j.solener.2014.05.042

31. Romero,M.A.B.(2011). Architecture of the place. A bioclimatic vision of sustainability in Brasilia. Nova Editorial Technique.

32. Rouse, J.W., Jr., Haas, R.H., Schell, J.A., & Deering, D.W. (1973, December 10-14). Monitoring Vegetation Systems in the Great Plains with ERTS [Paper Presentation]. The 3rd Earth Resource Technology Satellite-1 Symposium, Greenbelt, WA, USA.

33. Santamouris, M. (2015). Analyzing the heat island magnitude and characteristics in one hundred Asian and Australian cities and regions. Science of the Total Environment, 512-513, 582–598. https://doi.org/10.1016/j.scitotenv.2015.01.060

34. Snyder, W.C., Wan, Z., Zhang, Y., & Feng, Y.Z. (1998). Classification based emissivity for land surface temperature measurement from space. International Journal of Remote Sensing, 19(14), 2753-2774. https://doi.org/10.1080/014311698214497

35. Stathopoplou, M., Cartalis, C., & Petrakis, M. (2007). Integrating CORINE land cover data and Landsat TM for surface emissivity definitions: An application for the urban area of Athens, Greece. International Journal of Remote Sensing, 28(15), 2367–2393. https://doi.org/10.1080/01431160600993421

36. Taleghani, M., Crank, P., Mohegh, A., Sailor, D.J., Ban-Wess, G.A. (2019). The impact of heat mitigation strategies on the energy balance of a neighborhood in Los Angeles. Solar Energy, 177, 604-611. https://doi.org/10.1016/j.solener.2018.11.041

37. United States Geological Survey. (2019). Landsat 8 Data Users Handbook (LSDS-1574,Version 5.0). https://d9-wret.s3.us-west-2.amazonaws.com/assets/palladium/production/s3fs-public/atoms/files/LSDS-1574_L8_Data_Users_Handbook-v5.0.pdf

38. Voogt, J.A., & Oke, T.R. (2003). Thermal remote sensing of urban climates. Remote Sensing of Environment, 86(3), 370–384. https://doi.org/10.1016/S0034-4257(03)00079-8

39. Wang, R., Hou, H., Murayama, Y., & Morimoto, T.A. (2022). Three-dimensional Investigation of spatial relationship between building composition and surface urban heat island. Buildings, 12(8). https://doi.org/10.3390/buildings12081240

40. Weng, Q., & Fu, P. (2014). Modeling annual parameters of clear-sky land surface temperature variations and evaluating the impact of cloud cover using time series of Landsat TIR data. Remote Sensing of Environment, 140, 267–278. https://doi.org/10.1016/j.rse.2013.09.002

41. Weng, Q (2001). A remote sensing? GIS evaluation of urban expansion and its impact on surface temperature in the Zhujiang Delta, China. International Journal of Remote Sensing, 22(10), 1999–2014. https://doi.org/10.1080/713860788

42. World Population Review. (n.d). Lagos Population 2022. Retrieved 2022, from https://worldpopulationreview.com/world-cities/lagos-population

43. Xian, G. (2021). Monitoring and assessing urban heat island variations and effects in the United States. USGS Publications Warehouse. https://doi.org/10.3133/fs20213031

44. Yang, L., Qian, F., Song, D-X., & Zheng, K-J. (2016). Research on urban heat island effect. Procedia Engineering, 169, 11–18. https://doi.org/10.1016/j.proeng.2016.10.002

45. Zhou, D., Zhang, L., Hao, L., Sun, G., Liu, Y., & Zhu, C. (2016). Spatiotemporal trends of urban heat island effect along the urban development intensity gradient in China. Science of the Total Environment, 544, 617–626. https://doi.org/10.1016/j.scitotenv.2015.11.168

